

ARTICLE

DOI: 10.1038/s42004-018-0078-z

OPEN

Expanding heme-protein folding space using designed multi-heme β -sheet mini-proteins

Areetha D'Souza¹, Jaume Torres¹ & Surajit Bhattacharjya ¹

Nature has primarily exploited helical proteins, over β -sheets, for heme/multi-heme coordination. Understating of heme-protein structures has motivated the design of heme proteins utilizing coiled-coil helical structure. By contrast, de novo designed β -sheet proteins are less successful. However, designing proteins with discretely folded β -sheet structures encoding specific functions would have great potential for the development of new synthetic molecules e.g. enzymes, inhibitors. Here we report the design and characterization of multi-heme binding four-, six-, eight-, and twelve-stranded β -sheet mini-proteins (<40 amino acids) and proteins. Atomic-resolution structures demonstrate an expected β -sheet structural topology. The designed β -sheet mini-proteins pack or latch multiple hemes with high affinity in versatile orientations either by stacking or sideways, mimicking naturally occurring multi-heme protein conduits. The designed multi-stranded β -sheet heme proteins could serve as a platform for the generation of novel synthetic β -sheet protein mimics.

¹School of Biological Sciences, Nanyang Technological University, 60 Nanyang Drive, Singapore 637551, Singapore. Correspondence and requests for materials should be addressed to S.B. (email: surajit@ntu.edu.sg)

Although protein design has been successful in revealing interrelationship of sequences, structures, and stability^{1–5}, de novo designing of miniaturized proteins, <50 amino acids, with definite functions are challenging. This is because stability of the folded structures needs to be maintained by fewer interactions, and also active sites are to be designed within a small structural fold. However, miniaturized proteins are of substantial importance in therapeutics and biotechnology^{6–9}.

Heme as an active center in naturally occurring proteins performs multiple functions e.g. oxidation-reductions, electron transfer, energy harvesting, and gas exchange. Naturally occurring proteins are evolved to bind heme or multiple heme cofactors employing helical or helix-loop structural scaffolds. In-depth knowledge on heme-helical proteins has motivated toward designing of novel heme proteins.

Four helix coiled-coil structures were successfully designed that tightly bind heme along the long axis of helical assembly in aqueous solution and also in lipid membrane^{10–20}. The designed four helix coiled-coil or protein ‘maquettes’ ligate single heme or di-heme with bis-his coordination and have been engineered to carry out specific functions^{10,18,19}. Further, novel chemical functions based on heme-protein design, either on naturally occurring scaffolds or directed evolution, have been exploited^{21–23}.

There are only few naturally occurring β -sheet proteins that are known to bind heme using a large barrel structure^{24,25}. Notably, only limited progress has been achieved in designing miniaturized β -sheet proteins that would bind heme with high affinity akin to the naturally occurring proteins^{26–28}. The functional attributes of heme are largely regulated by the protein matrix and surrounding amino-acid residues; therefore, designed heme- β -sheet proteins would be important to garner new applications^{21–23}. β -sheet protein designed, de novo, is largely limited to β -hairpins, and three- or four-stranded β -sheet structures as models of folding of β -sheet proteins^{29–32} and aggregated β -sheets^{33,34}. Furthermore, designing of multi-stranded β -sheet proteins could be challenging due to aggregation and insolubility in aqueous solution. Recently, we reported designed ‘heme-cage’ β -sheet mini proteins that bind to single heme, using bis-his coordination, at high affinity in four-stranded β -sheet topology²⁸.

Here, we design and characterize water soluble mini-proteins and several variants that fold into multi-stranded antiparallel β -sheet structures, and coordinate two- or four-heme molecules. The construction of multi-stranded functional β -sheet mini-proteins, and proteins reported in this work may have implications for developing synthetic proteins.

Results

Design of mini-proteins. In nature, proteins can accommodate multiple hemes, and di-heme helical proteins are designed^{10,11,15,16}. Multi-heme cytochromes ligate many heme molecules in close proximity for efficient electron transport and enzymatic activity. MtrF, an outer member cytochrome, bind 10 heme groups using stacking and side-wise packing orientation forming a conduit (Supplementary Fig. 1). An important step toward designing functional protein conduits would be to develop synthetic proteins that are able to engage multiple-heme molecules with high affinity. However, it remains obscure how multiple-heme molecules can be coordinated within a minimal β -sheet structure.

Towards this goal, we have designed water soluble mini-proteins and several variants that are expected to fold into multi-stranded antiparallel β -sheet structures and coordinate with two- or four-heme molecules (Fig. 1). Previously, we reported a hydrophobic peptide, termed peptide-7, that assumes a

K ^L -I-F-W- ^D P-G-H-F-V- η -aminooctanoic acid-T-Y-H- ^D P-G-H-M-V- η -aminooctanoic acid-V-T-H- ^D P-G-T-F-I-K ²⁸	Mini-protein1
K ^L -I-T-Y-V-F-W- ^D P-G-H-F-I-T-H-T- η -aminooctanoic acid-V-H-Y-M-V-H- ^D P-G-Y-T-I-L-T-K ³⁰	Mini-protein2
K ^L -I-F-W- ^D P-G-H-F-V- η -aminooctanoic acid-T-Y-H- ^D P-G-H-M-V- η -aminooctanoic acid-V-T-H- ^D P-G-C-F-I-K ²⁸	Mini-protein3
K ^L -I-T-Y-V-F-W- ^D P-G-H-F-I-T-H-T- η -aminooctanoic acid-V-H-Y-M-V-H- ^D P-G-C-T-I-L-T-K ³⁰	Mini-protein4
K ^L -I-F-W-P-G-H-F-V- η -aminooctanoic acid-T-Y-H-P-G-H-M-V- η -aminooctanoic acid-V-T-H-P-G-T-F-I-K ²⁸	Mini-protein5
K ^L -I-F-W- ^D P-G-H-F-V- η -aminooctanoic acid-T-Y-H- ^D P-G-T-M-V- η -aminooctanoic acid-V-T-S- ^D P-G-C-F-I-K ²⁸	Mini-protein6
K ^L -I-T-Y-V-F-W- ^D P-G-H-F-I-T-H-T- η -aminooctanoic acid-V-S-Y-M-V-S- ^D P-G-Y-T-I-L-T-K ³⁰	Mini-protein7

Fig. 1 Primary structures of designed mini-proteins and variants. Heme coordinating His residues are highlighted in red. The histidine residues in mini-protein2 are replaced to serine and threonine (blue) in mini-protein6. Two histidine residues of mini-protein3 in β -strand2 are replaced to serine (blue) in mini-protein7

six-stranded β -sheet structure and bind to di-heme with low affinity, $K_d \sim 0.4 \mu\text{M}$, in detergent micelle solution²⁷. The primary structure of mini-protein1 has been constructed by replacing hydrophobic residues with polar and cationic residues of peptide-7 to increase aqueous solubility. The mini-protein1 would form six-stranded β -sheet structure and may coordinate di-heme in a sidewise packing using bis-his coordination. In particular, sidechains of residues H7 and H13, between β -strands 2 and 3, and residues H16 and H22, between β -strands 4 and 5, would bind two heme.

The 30-residue mini-protein2 is designed to assume a four-stranded longer- β -sheet structure that can ligate two heme in a stacking orientation. The sidechains of residues H10/H18 and H14/H22 from the adjacent β -strands 2 and 3 would form the binding pocket for two heme coordination. Mini-protein3 and mini-protein4 are Cys variants of mini-protein1 and mini-protein2 that are able to form homo dimers through S-S bond formation. Mini-protein3 would bind to an array of four-heme molecules in a twelve-stranded β -sheet topology, whereas mini-protein4 would coordinate with four-heme molecules within eight-stranded β -sheet structures. Residues D-Pro-Gly and cross-strand aromatic packing are anticipated to stabilize the designed multi-stranded β -sheet fold^{31,32,35}. The hydrophobic heme binding pockets in the designed mini-proteins are maintained by bis-his coordination and η -aminooctanoic acid between the adjacent β -strands^{27,28}. In addition, in order to correlate heme binding affinity and β -sheet structures, mini-proteins5, 6, and 7 were prepared.

Structures and heme binding of mini-protein1 and variants.

Designing β -sheet proteins often encountered challenges of aggregation and oligomerization. Pulse field gradient (PFG) NMR was used to assess potential oligomerization of designed mini-proteins 1, 2, 3, and 4 in aqueous solution. Designed mini-proteins showed an expected molecular weight (MW) akin to the monomeric state (Supplementary Table 1). Analyses of two-dimensional NOESY spectra demonstrated diagnostic long-range, backbone/backbone, and backbone/sidechain NOE connectives (Fig. 2a, Supplementary Fig. 2a). Further, ¹H α and ¹³C α secondary chemical shift values supported a mini-protein1 assumed six-stranded β -sheet structure (Supplementary Fig. 2b).

An ensemble of structures of mini-protein1 was determined by CYANA, using 462 NOE-driven distant constraints (Fig. 2b, Supplementary Table 2). The backbone and all heavy atom

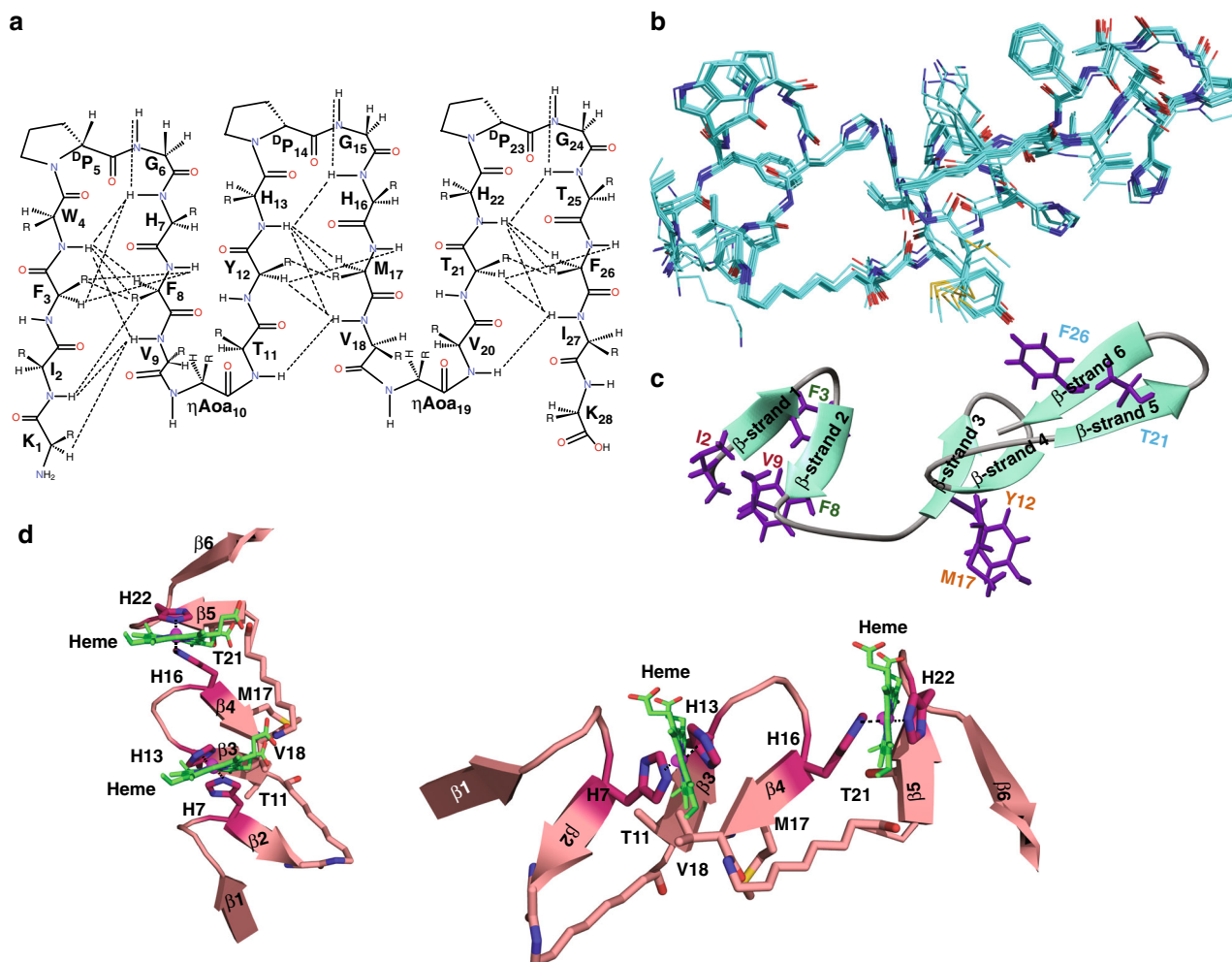


Fig. 2 NMR derived structure of mini-protein1. **a** Schematic representation of some of the diagnostic NOEs, dotted line, observed in mini-protein1. **b** Superimposed ten low-energy structures of mini-protein1. **c** Packing interactions observed within β -sheets: I2/V9 (magenta), F3/F8 (blue) between β -strands 1 and 2II, M17/Y12 (orange) between β -strands 3 and 4, and F26/T21 (green) between β -strands 5 and strand 6. **d** Model of mini-protein1/heme complex

RMSD values of the structural ensemble were estimated to be 0.28 Å and 0.66 Å, respectively (Supplementary Table 2). The 3-D structure of the 28-residue-long mini-protein1 is defined by six β -strands, β -strand 1: residues I2-W3, β -strand 2: residues H7-V9, β -strand 3: residues T11-H13, β -strand 4: residues H16-V18, β -strand 5: residues V20-H22, and β -strand 6: residues T25-I27 (Fig. 2c). The $^{\text{D}}\text{P}$ -G residues form type II' β -turns (Fig. 2c). Further, sidechain/sidechain cross strand packing can be seen among residues F3/F8, I2/V9, Y12/M17, and T21/F26 potentially stabilizing the fold (Fig. 2c). Cross-strands packing interactions were more limited between β -strands 2 and 3, and 4 and 5, at the two heme binding pockets, due to extended conformations of η -aminooctanoic acid (Fig. 2c). In other words, the topology mini-protein1 can also be described as three pairs of antiparallel β -sheets connected by linkers. NMR and chemical shift analyses of the S-S bonded mini-protein3 delineated a symmetric homodimer forming a twelve-stranded β -sheet structure (Supplementary Fig. 3).

UV-Vis absorption spectra of heme were utilized to estimate heme-binding affinity and binding stoichiometry of the designed mini-proteins. Figure 3 summarizes heme binding of the mini-protein1 and mini-protein3. Absorption spectra of heme were acquired at different molar ratios of mini-proteins 1 and 3

(Figs. 3a, b). Mini-proteins are ligated to heme, as evident from the shift of the Soret band to 414 nm from a broad band consisting of \sim 398 nm of free heme. The Soret band of mini-proteins/heme complex appeared highly intense along with low-intensity α and β bands from 530 to 560 nm (Supplementary Table 3). The heme absorption changes at 414 nm are plotted as a function of mini-proteins/heme ratios (Fig. 3b, e) indicating high-affinity saturable binding. Reduction of heme/mini-protein complexes by sodium dithionite had caused a red shift, 428 nm, and more resolved α and β bands (Supplementary Figs. 4b and 4d, Supplementary Table 3). These spectral features of heme are diagnostics of bis-his ligation, wherein heme occupies a hexacoordinated low-spin state of Fe(III) center^{36,37}.

The heme-binding affinity of the designed mini-proteins were quantified by titrating heme against a fixed concentration of mini-proteins (materials and methods). The heme-binding isotherms demonstrated high-affinity heme/mini-protein complexes with a clear break point at the stoichiometric concentration of heme (Fig. 3c, f, Table 1). As estimated from Job's plots, the six-stranded mini-protein1 binds to two heme, whereas the twelve-stranded mini-protein3 ligated to four-heme molecules at the heme-binding pockets (Supplementary Figs. 4a and 4c). Plausible model of heme complex of mini-proteins1 is shown in

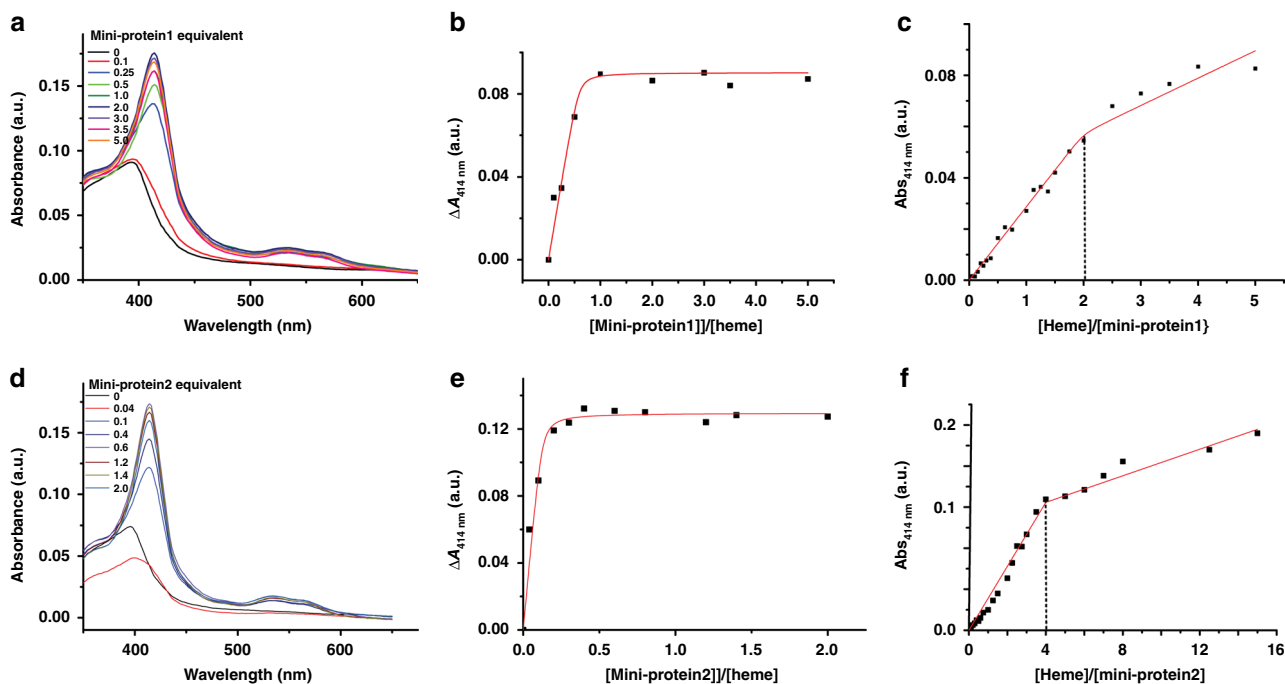


Fig. 3 Heme binding characterisation of mini-protein1 and 3. **a** Absorption changes of heme (10 μM) on titrating mini-protein1 (0-5 equivalents) and **b** peptide titration curve monitoring absorbance changes in Soret maximum (414 nm). **c** Heme-binding isotherm of mini-protein1 (4 μM) shows a breakpoint at stoichiometry 2 heme/1 peptide. **d** Absorption changes of heme on titrating mini-protein3 (0-2 equivalents). **e** peptide titration curve monitoring absorbance changes at Soret maximum (414 nm). **f** Heme-binding isotherm of mini-protein1 (4 μM) shows a break point at stoichiometry 4 heme/1 peptide

Table 1 Dissociation constant (K_d) values and peroxidase ability of designed mini-proteins with heme

Mini-protein	K_d	kcat/KM ($10^3\text{M}^{-1}\text{s}^{-1}$)
1	5.39 ± 2.1 nM	0.54
2	1.61 ± 0.13 nM	0.77
3	<1 pM	Low
4	<1 pM	Low
5	0.78 ± 0.95 μM	1.23
6_{red}	1.34 ± 8 pM	ND
6_{ox}	<1pM	ND
7	3.2 ± 0.8 μM	ND
MP-8	ND	10506.1
Myoglobin	ND	131.8
Cytchrome C	ND	Low

ND not determined

Fig. 2d. The heme-binding topology of the β -sheet mini-proteins is in contrast to the designed di-heme helical proteins, where cofactors occupy a stacked orientation.

In order to correlate β -sheet structures and heme-binding affinity, residue D-Pro at 5, 14, and 24 positions in mini-protein1 was replaced by L-Pro in mini-protein5 (Fig. 1). NMR analyses revealed that mini-protein5 is largely unfolded in solution (Supplementary Fig. 5). Heme binding studies showed that mini-protein5 binds to heme with appreciably low affinity, $K_d \sim 0.78$ μM (Supplementary Fig. 6, Table 1). Heme-binding isotherm showed continuous increase in heme absorption without a clear break-point indicating a low-affinity complex formation (Supplementary Fig. 6b).

Further, in order to decipher any co-operativity among heme-binding pockets, heme-ligating residues, H16 at β -strand4 and S22 at β -strand5, at the distal binding pocket were replaced to Thr

and Ser, respectively, in mini-protein6 (Fig. 1). Heme-binding analyses, binding isotherms and Job's plots delineated that mini-protein6 can coordinate tightly either with a single heme, in reduced (Cys) form, or binds to di-heme in an oxidized (S-S) state (Table 1, Supplementary Fig. 7). The independent heme ligation at the designated binding pockets strongly indicated that the unoccupied binding sites can potentially be engineered for the further designing of heme-containing multifunctional β -sheet proteins.

Structures and heme binding of mini-protein2 and variants.

Secondary chemical shift of $^1\text{H}\alpha$ and $^{13}\text{C}\alpha$ of individual residues (Supplementary Fig. 8b) and diagnostic inter-strands NOE connectivity (Fig. 4a, Supplementary Fig. 8a), demonstrated that mini-protein2 folds into populated four-stranded β -sheet structure, as per the design, in aqueous solution. Figure 4b shows an ensemble of superposed structures of the designed mini-protein2 determined using 387 NOE driven distance constraints. The 3-D structure of the mini-protein2 was well resolved with backbone and sidechain RMSDs of 0.34 and 0.68 \AA , respectively (Supplementary Table 2).

The four-stranded β -sheet topology of mini-protein2 is defined by β -strand 1: residues T3-W7, β -strand 2: residues H10-H14, β -strand 3: H18-H22, and β -strand 4: Y25-T29, whereas central $^{\text{D}}\text{P-G}$ motifs assumed type II' β -turn (Fig. 4c). The η -aminooctanoic acid residue was in extended conformations, causing diminished interactions between β -strands 2 and 3, of the heme-binding pocket. Due to the two-fold symmetry, NMR spectra of S-S linked homo-dimeric mini-protein4 showed one set of signals from residues (Supplementary Fig. 9a). Secondary chemical shift was akin to the four-stranded β -sheet structure for each subunit (Supplementary Fig. 9b).

In UV-Vis absorption studies of heme showed a red-shifted Soret band, λ_{max} 414 nm, and low-intense α , β bands ~ 530 and

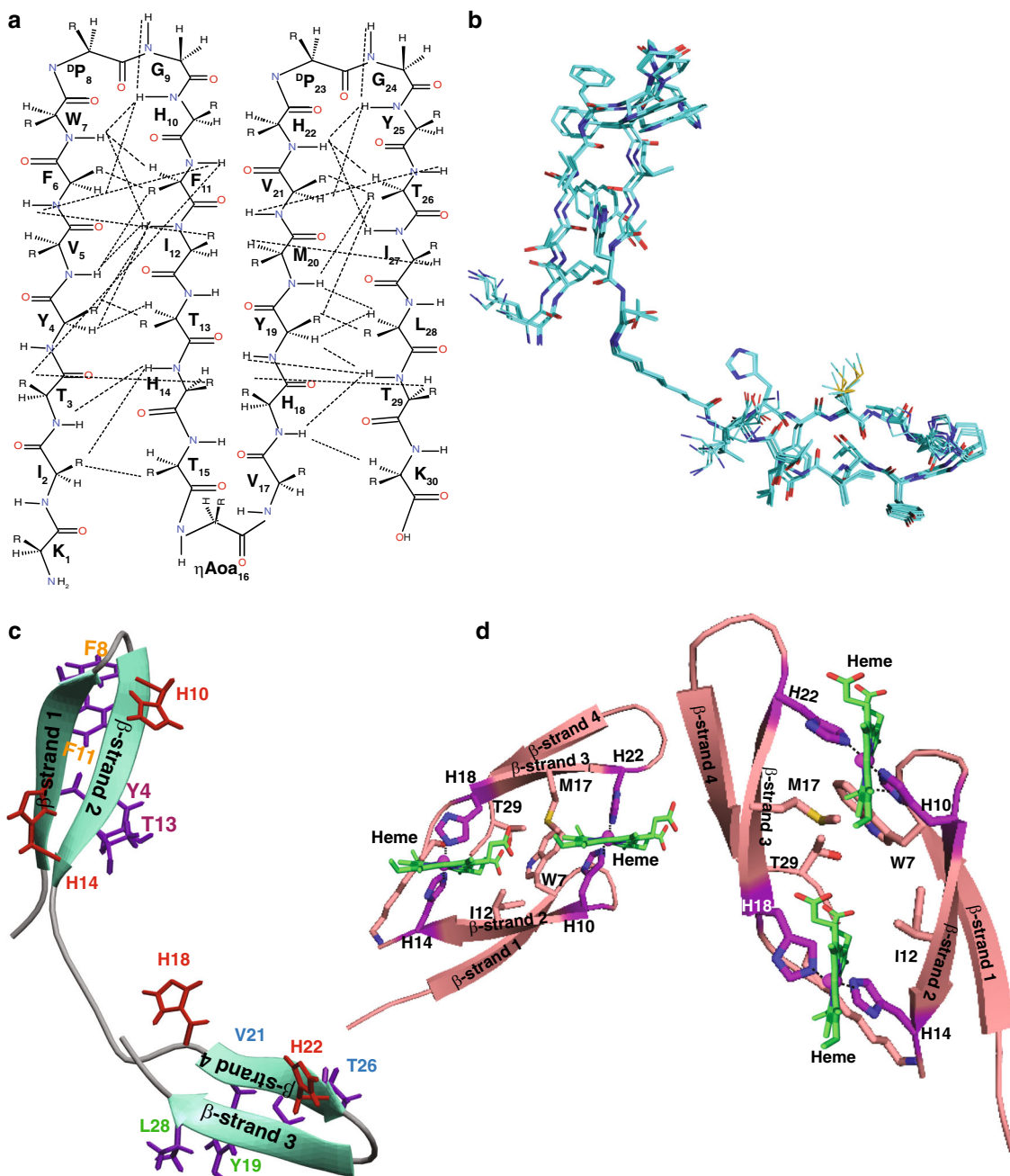


Fig. 4 NMR derived structure of mini-protein3. **a** Schematic representation of diagnostic NOEs, dotted line observed in mini-protein3. **b** Superimposed ten low-energy structures of mini-protein3. **c** Packing interactions observed within β -sheets: Y4/T13 (magenta), F3/F8 (orange) between β -strands 1 and 2, Y19/L28 (green) and V21/T26 (blue) between β -strands 3 and 4. The four heme coordinating His residues are highlighted (red). **d** Model of mini-protein2/heme complex

560 nm upon titrations with mini-proteins2 and 4 (Fig. 5a, d, Supplementary Table 3) and dithionite reduction of heme-protein complexes (Supplementary Figs. 10b, 10d), indicating bis-his ligation of heme-protein complexes. High-affinity heme binding has been maintained by mini-protein2 and the S-S bonded variant mini-protein4 (Fig. 5b, e). Job's plots clearly demonstrated that the mini-protein2 and mini-protein4 were ligated to the desired two- and four-heme molecules (Supplementary Figs. 10a, 10c). Binding isotherms delineated that heme binds with high affinity, $K_d \sim \text{nM-pM}$, to the designed mini-proteins2 and 4 (Fig. 5c, f, Table 1). A model of heme/mini-protein2 complex was derived from the apo-structure highlighting two-heme molecules

ligated with bis-his coordination at the binding pocket in a stacking orientation (Fig. 4d).

Further, in order to assess binding of di-heme at the binding pocket, His residues (H18 and H22) in the β -strand3 were replaced to Ser in mini-protein7 (Fig. 1). UV-Vis absorption spectra, binding isotherms, and sodium dithionite reduction experiments demonstrate that mini-protein7 interacted with heme with a significantly lower affinity, $K_d \sim 3.2 \mu\text{M}$ (Table 1, Supplementary Fig. 11). These data strongly suggested that high-affinity di-heme binding would require His residues at the β -strand2 and β -strand3 in the binding pocket.

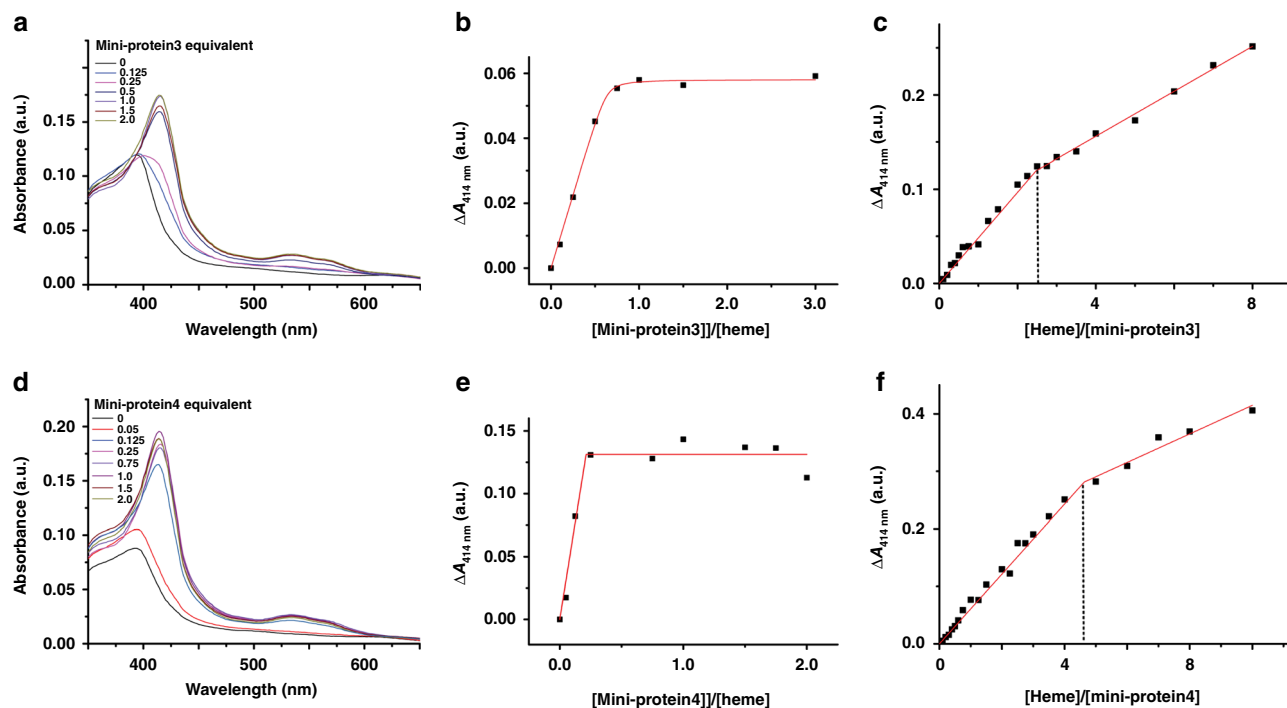


Fig. 5 Heme-binding characterization of mini-protein2 and 4. **a** Absorption changes of heme (10 μ M) on titrating mini-protein2 (0–2 equivalents). **b** Peptide titration curve monitoring absorbance changes in Soret maximum (414 nm). **c** Heme-binding isotherm of mini-protein2 (10 μ M) shows a break point at stoichiometry 2 heme/1 peptide. **d** Absorption changes of heme on titrating mini-protein4 (0–2 equivalents). **e** Peptide titration curve monitoring absorbance changes at Soret maximum (414 nm). **f** Heme-binding isotherm of mini-protein4 (10 μ M) shows a break point at stoichiometry 4 heme/1 peptide

Heme complex and stability of designed mini-proteins. Global conformational changes, stability, and folding of apo and holo proteins were investigated by CD, FTIR, and UV–Vis spectroscopy methods. Far UV CD spectra of mini-proteins 1, 2, 3, and 4 were characterized by an intense negative dichroic band at \sim 210–212 nm, akin to β -sheet conformations (Supplementary Fig. 12, a–d). CD spectra of the holo mini-proteins were largely similar to the apo forms, while CD bands were somewhat shifted to 216 nm for mini-proteins 2, 3, and 4 (Supplementary Fig. 12, a–d), due to a better packing of heme/protein complexes. CD spectra of the cofactor in holo mini-proteins revealed a signal at 400–414 nm, indicating a chiral environment of heme in the complex (Supplementary Fig. 12, inset).

IR spectra of apo and holo mini-proteins 1, 2, 3, and 4 were obtained in D_2O (Supplementary Fig. 13). In all cases, the amide-I band showed two clear features before addition of heme. The first is centered at \sim 1671 cm^{-1} and is assigned to β -turns. This band did not shift for any of the mini-proteins after addition of heme. The second feature appears in the range 1639–1645 cm^{-1} that is attributed to β -sheet structures. This band shows a shift to lower frequency after addition of heme.

Heme ligation stability of the designed mini-proteins were further investigated by acquiring UV–Vis heme spectra at various concentrations of urea, a chemical denaturant (Supplementary Fig. 14, a–f). Figure 6a shows a change of wavelength of the Soret peak (λ_{max}) of heme-mini-proteins complexes as a function of urea concentrations. Remarkably, the designed mini-proteins, 1, 2, 3, and 4, were able to ligate heme even at 6 to 8 M urea concentration. On the other hand, heme ligation to mini-protein5 appeared to be destabilized at a much lower concentration of urea. Note, a lower affinity of interactions has been estimated for the mini-protein5 to heme (Table 1). Collectively, both the holo and apo forms of the mini-proteins retained similar β -sheet conformations albeit certain conformational changes were

observed in complex with heme. Heme complexed with mini-proteins demonstrated extremely high stability against denaturation.

Peroxidase activity of the designed mini-proteins. Designed heme proteins can act as peroxidases^{11,14,16,26}. Figure 6b shows the time course of oxidation of a chromogenic substrate ABTS at a fixed concentration of H_2O_2 by the designed mini-proteins. The k_{cat}/K_M values, derived from Michaelis–Menten equation, of ABTS oxidation of the designed mini-proteins are listed in Table 1. As seen, di-heme binding mini-proteins 1 and 2 showed peroxidase like activity more than heme alone (Fig. 6b). Interestingly, ABTS oxidation kinetics of the S-S linked mini-proteins 3 and 4, binding to four heme moieties, were found to be comparable to the free heme (Fig. 6b). By contrast mini-protein5, coordinating two heme with low affinity (Table 1), delineated a faster kinetics of substrate oxidation (Fig. 6b) and a higher- k_{cat}/K_M value (Table 1). Note, peroxidase or enzymatic activity of heme-containing proteins is determined by the axial ligands coordination of heme Fe (III) atom^{27–29}. A lower-peroxidase activity is expected to occur where Fe (III) of heme is strongly ligated to the axial ligands. On the other hand, a higher peroxidase activity implies a lower-affinity interaction of the axial ligands with Fe (III) of heme or unoccupied Fe (III) atom, e.g. penta-coordinated heme system^{38–40}.

To better correlate heme coordination and enzymatic action, we estimated peroxidase activity of naturally occurring heme proteins myoglobin, cytochrome C, and micro-peroxidase peptide 8 or MP8 (Table 1, Supplementary Fig. 15). Myoglobin and MP8, penta-coordinated heme proteins, demonstrated higher-peroxidase activity compared to the designed mini-proteins. By contrast, peroxidase activity of cytochrome C, hexa-coordinated heme protein was found to be appreciably limited

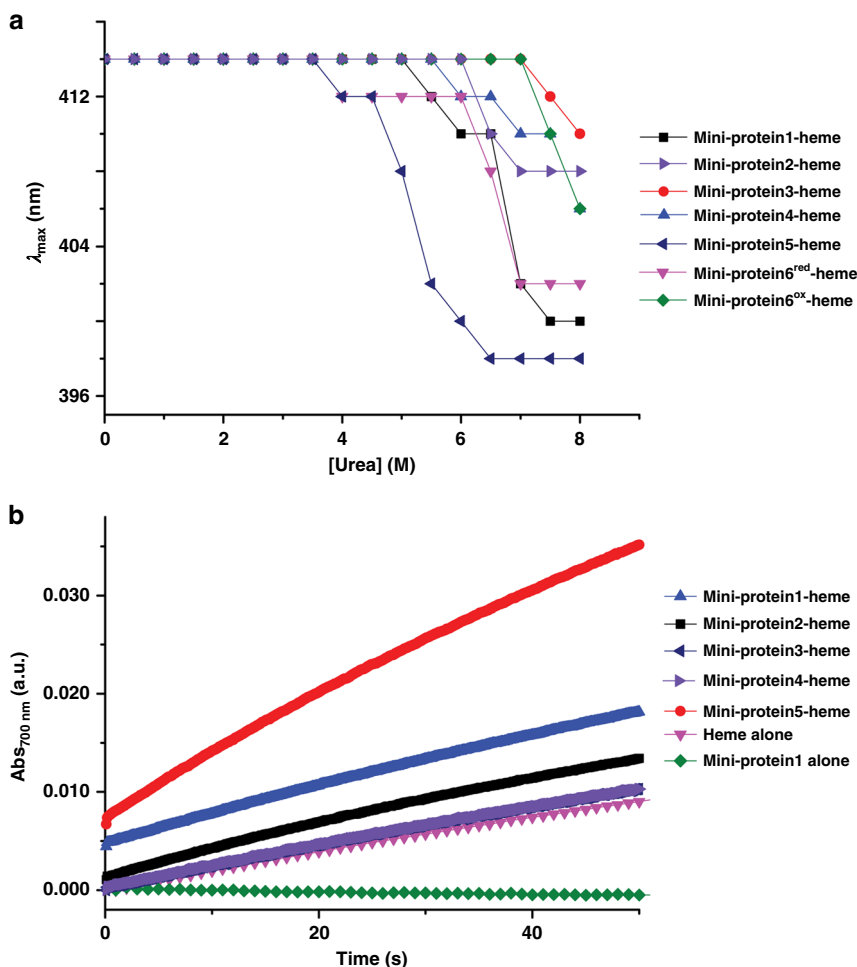


Fig. 6 Peroxidase and stability of the mini-proteins. **a** Changes of wavelength of heme λ_{\max} of mini-protein/heme complexes upon titration with urea. **b** ABTS oxidation at 700 nm as a function of time for the mini-protein/heme complexes at 20 mM H_2O_2 concentration

(Supplementary Fig. 15). Thus, poor peroxidase activity of the designed mini-proteins suggested that the active centre, Fe atom of heme, is strongly ligated to the two axial ligands or histidine residues of mini-proteins that correlates well with the low- K_d values of heme/mini-protein complexes (Table 1).

Discussion

Naturally occurring larger proteins can tightly coordinate multiple-heme molecules in a spatial proximity for efficient electron transfer within heme conduit and other activities. The incorporation of multiple heme into a miniaturized protein scaffold could be highly challenging. The current work demonstrates design of multi-stranded β -sheet mini-proteins that are able to coordinate di- and tetra-heme molecules with high affinities. The multi heme/protein complexes may inform the development of synthetic functional molecules including therapeutics.

Methods

Materials. Mini-proteins were commercially obtained from GL-Biochem (Shanghai, China)TM. D_2O and 4, 4-dimethyl-4-silapentane-1-sulfonic acid (DSS) were purchased from Cambridge Isotope Laboratories Inc. (Massachusetts, USA). Other chemicals including sodium dithionite, hemin, cytochrome C, myoglobin, H_2O_2 , and ABTS were purchased from Sigma-Aldrich.

Purification of crude peptides. Synthetic mini-proteins were purified by use of reverse-phase HPLC using C_{18} or C_4 of 300 Å pore size, 5 μM particle size. A linear solvent gradient 10–90% of acetonitrile/water (both solutions containing 0.1% v/v

TFA) was used to elute the samples at a flow rate of 2 ml/min. The major elute peak fractions obtained were collected, lyophilized, and confirmed using MALDI-TOF mass spectrometry.

Preparation of heme. A 2.5 mM stock solution of heme (by weight) was freshly prepared in 0.1% NaOH in milliQ water and stored under dark. The working stock of heme was prepared by double dilution with the buffer of required pH. The concentration of heme stock was further estimated using the pyridine hemochrome assay.

Preparation of disulfide-linked mini-protein samples. Cysteine variants of purified mini-proteins (approx. 2 mg lyophilized powder) were treated with 50% DMSO, pH 7.0 and kept in the dark for around 24 h. The mini-proteins were lyophilized to remove excess DMSO. The oxidized peptide samples were then purified using HPLC and lyophilized.

Preparation of MP-8. Horse heart cytochrome C (~10 mg) and pepsin ~1 mg were dissolved in 1 ml double-distilled water. The pH of the solution was adjusted to 2.0 and kept for 24 h at room temperature. The sample was diluted in 10% acetonitrile and 0.1% TFA, and purified by HPLC with an acetonitrile linear gradient of 10–60% at 1 ml/min flow rate using a C_{18} column (300 Å pore size, 5 μM particle size). The major peak obtained by HPLC purification was lyophilized and further treated with ~1 mg trypsin in 1 ml water. The pH of the solution was adjusted to 8.5 and kept for 24 h at room temperature. The sample was diluted in 10% acetonitrile and 0.1% TFA, and purified by HPLC using a linear acetonitrile gradient of 10–60% acetonitrile at 1 ml/min flow rate using a C_{18} column. The major peak obtained by HPLC purification (MP-8) was lyophilized and confirmed using mass spectrometry.

UV-Vis studies. For the mini-proteins, the heme binding affinity was characterized using a multi-well plate reader (Tecan Infinite M200 PRO) by titrating increasing concentrations of mini-proteins (upto five equivalents) to a fixed

concentration of heme prepared in 5 mM Tris pH 9.0. The Soret band intensity at 414 nm was monitored for holo mini-proteins formation for each aliquot after three hours of incubation. Wavelength scans from 350–600 nm was further recorded to monitor the shift in the absorption maxima of heme on binding to the designed mini-proteins. Also, a fixed concentration of mini-proteins, in 5 mM Tris-HCl buffer at room temperature, was titrated with increasing concentrations of heme (upto 5 stoichiometric equivalents) monitoring the Soret region (350–650 nm). The K_d values were estimated by plotting absorbance at λ_{max} (414 nm) versus heme concentration using the equation (1) for high-affinity heme binding. Each binding experiment was performed at least three independent times and reported errors are standard deviations from the mean.

$$\Delta A = H_t \epsilon_{free} + (\epsilon_{bound} - \epsilon_{free}) \frac{([H_t] + n[P_t] + K_{d,app}) - \sqrt{([H_t] + n[P_t] + K_{d,app})^2 - 4[H_t]n[P_t]}}{2} \quad (1)$$

where $[H_t]$ is the total heme concentration, $[P_t]$ is the total peptide concentration, $K_{d,app}$ is the apparent dissociation constant, ϵ_{free} is the extinction coefficients of free heme, ϵ_{bound} is the extinction coefficients of bound heme, n is the number of binding sites, and ΔA is the change in absorbance at a given heme concentration.

Heme stoichiometry was determined using method of continuous variation or Job's plot. Typically, mini-protein samples at 100 μ M concentration and heme stocks were prepared in 5 mM Tris-HCl buffer, pH 9.0. Different ratios of the two stock solutions were mixed, while keeping the total volume constant. The absorbance values at 414 and 356 nm were recorded for the various mole fractions of heme using a multi-well plate reader (Tecan Infinite M200 PRO). This difference in absorbance was then analyzed using the mole fraction of heme. The bound and free heme-extinction coefficients were determined by obtaining the absorption spectra at varied concentrations of mini-proteins heme (pre-incubated for an hour at their respective stoichiometry) / free heme. The λ_{max} values were then plotted against the concentration of heme to generate the extinction coefficients.

The ferrous or reduced heme spectra were obtained by the addition of sodium dithionite (from a freshly prepared 5 mM stock solution) to the mini-proteins-heme complex (20 μ M mini-proteins, heme concentration) in 5 mM Tris-HCl, pH 9.0, buffer (de-aerated for 30 minutes by purging nitrogen). For urea stability studies, increasing concentrations of urea (0–8 M) were titrated into a 10 μ M mini-protein/heme solutions (stoichiometric amount of heme) containing 5 mM Tris, pH 9.0. The mini-protein/heme samples were equilibrated for 3 h at room temperature at required urea concentration. The Soret region (350–650 nm) was monitored spectrophotometrically using a multi-well plate reader to observe the changes in the Soret maxima on increasing concentrations of the denaturant.

Peroxidase activity studies. A SX20 stopped flow spectrophotometer (Applied Photophysics) was used to monitor the peroxidase dependent oxidation of ABTS substrate. The oxidation of ABTS, as a measure of peroxidase activity, was recorded at 700 nm versus time at room temperature. 8 μ M of mini-protein samples or naturally occurring protein samples (myoglobin, cyt C, MP-8) containing 1 μ M heme and 5 mM ABTS were mixed with 20 mM hydrogen peroxide in 5 mM Tris, pH 9.0. The absorbance values at 700 nm was converted to concentration ($\epsilon_{700nm} = 1.6 \times 10^4 \text{ M}^{-1}\text{cm}^{-1}$) and the reaction rate was calculated by linear-regression analysis. In-order to obtain the kinetic parameters for the mini-protein/heme complexes and naturally occurring proteins (V_{max} , K_m , k_{cat}/K_m), reaction rates were obtained by varying hydrogen peroxide concentrations. These reaction rates were analyzed versus H_2O_2 concentration and fitted to the Michaelis–Menten equation.

$$V = \frac{V_{max}[\text{H}_2\text{O}_2]}{K_m + [\text{H}_2\text{O}_2]} \quad (2)$$

V is the reaction rate ($\mu\text{M/s}$), V_{max} is the maximal velocity for the enzymatic reaction ($\mu\text{M/s}$), K_m is the Michaelis–Menten constant and $[\text{H}_2\text{O}_2]$ is the concentration of H_2O_2 used. Turnover numbers (k_{cat}) were calculated by dividing the maximal velocity V_{max} by the concentration of heme-peptide complex (0.5 μM).

Circular dichroism studies. Apo and holo peptide solutions (10 μM) were prepared in 5 mM Tris buffer, pH 9.0. Far-UV circular dichroism (CD) studies (JASCO) were performed using a 1 cm-path-length cuvette with a 1 nm bandwidth and a step size of 0.5 nm at 0.5 seconds per data set. CD spectra were also recorded in the Soret region (350–450 nm) to monitor heme environment for the heme-peptide complexes at a 1 nm bandwidth and a step size of 0.5 nm at 0.5 seconds per data set.

NMR spectroscopy. NMR experiments were performed at 278 K on a Bruker DRX 600 MHz or 700-MHz spectrometer equipped with a cryo-probe. The samples were prepared by dissolving lyophilized powder of mini-proteins (0.25 mM concentration) in 500 μL 90% $\text{H}_2\text{O}/10\%$ D_2O and adjusting the pH to 5.5. Homonuclear ^1H - ^1H 2-D TOCSY (mixing time-80 ms) and NOESY (mixing time-200 ms) experiments were carried out for sequence-specific resonance assignments. The experiments were recorded using 64 scans, with spectral widths of 13 ppm in F1 and F2

direction, and using 2048 x 350 data points. NMR data were processed using TopSpin 2.1 (Bruker), and the chemical shifts were referenced directly (^1H) to the frequency of DSS. Natural abundance ^{13}C - ^1H HSQC experiments were carried out by dissolving lyophilized peptides in 100% D_2O and ^{13}C chemical shift was referenced indirectly from the ^1H frequency of DSS.

To estimate diffusion coefficient, DOSY-NMR experiments were carried out. 0.25 mM concentration of mini-proteins and 0.1 mM of DSS was prepared in 99% D_2O solution, and were recorded on a Bruker DRX 700-MHz spectrometer equipped with a cryo-probe at 278 K. The pulse sequence was a stimulated echo bipolar gradient pulse (stebppg1s) with the DOSY spectra acquired for each sample using a 5–95% gradient having 16 increments (exponential array), linear ramp, diffusion gradient length (δ) 1.5 ms, and big delta (Δ) 180.0 ms. MWs were estimated by a further extrapolation of the Stokes–Einstein equation assuming a spherical shape of the peptide.

Structure calculation. Ensembles of 3-D structures of peptides were calculated, using CYANA 2.1, from NOE-driven distance constraints and backbone dihedral angle (ϕ , ψ) constraints. Based on intensity, NOE cross-peaks observed in the 2-D NOESY spectra were categorized into strong, medium, and weak and further translated to upper bound distance constraints between 2.5–5.0 Å. Backbone dihedral constraints were obtained from PREDITOR-WISHART server based on the secondary chemical shifts of αH and NH protons. The NOE restraints and predicted dihedral angles values were used to carry out several rounds of structure calculations. Of the 100 structures generated, 20 low-energy structures were selected for evaluation and analyses. PROCHECK-NMR was used to assess the stereo-chemical quality of the structure ensembles. The structures are analyzed visually by PYMOL, MOLMOL, and INSIGHTII. For deriving models of mini-proteins/heme complexes, sidechains of heme coordinating His residues were brought into proximity by adjusting distances using CYANA. Distance constraints were assigned between the $\text{Ne}2$ of histidine pairs. Heme b pdb coordinates were inserted to the structure and the models were prepared using PYMOL.

FT-IR spectroscopy. FT-IR spectra were recorded on a Nicolet Nexus 560 spectrometer (Madison, USA) purged with N_2 and equipped with a MCT/A detector cooled with liquid nitrogen. Attenuated total reflection (ATR) spectra were measured with a 20-reflections HATR accessory (PIKE Technologies, Madison, WI). Approximately 100 μL of a D_2O solution of mini-proteins alone (apo) or in the presence of heme (holo) were applied onto a 45° trapezoidal (80 x 10 x 2 mm) ZnSe internal reflection element (IRE), with $<1 \mu\text{m}$ penetration depth at a wavelength of 6 μm . Immediately after deposition of the liquid sample, 200 scans were collected at a resolution of 4 cm^{-1} , averaged and processed with one-point zero filling and Happ–Genzel apodisation. A spectrum of buffer in D_2O was collected in the same conditions and subtracted from each sample. Percentages of secondary structure were estimated by fitting the amide I region (from 1700 to 1600 cm^{-1}) after mild Fourier deconvolution. The amide I band was Fourier self-deconvolved (FSD) using a full-width at a half-height (FWHH) of 23 cm^{-1} and an enhancement factor, k , of 1.8.

Data availability

The authors declare that all data supporting the findings of this study are available within the article and its Supplementary Information files or from the corresponding authors upon reasonable request.

Received: 25 July 2018 Accepted: 16 October 2018

Published online: 05 November 2018

References

- Chevalier, A. et al. Massively parallel de novo protein design for targeted therapeutics. *Nature* **550**, 74–79 (2017).
- Rocklin, G. J. et al. Global analysis of protein folding using massively parallel design, synthesis, and testing. *Science* **357**, 168–175 (2017).
- Lu, Y., Yeung, N., Sieracki, N. & Marshall, N. M. Design of functional metalloproteins. *Nature* **460**, 855–862 (2009).
- Lapidoth, G. et al. Highly active enzymes by automated combinatorial backbone assembly and sequence design. *Nat. Commun.* **9**, 2780 (2018).
- Lu, P. et al. Accurate computational design of multipass transmembrane proteins. *Science* **359**, 1042–1046 (2018).
- Hosseinzadeh, P. et al. Comprehensive computational design of ordered peptide macrocycles. *Science* **358**, 1461–1466 (2017).
- Rodríguez, J. et al. DNA-binding miniproteins based on zinc fingers. Assessment of the interaction using nanopores. *Chem. Sci.* **9**, 4118–4123 (2018).
- Anderson, J. M. & Andersen, N. H. A pH switch for β -sheet protein folding. *Angew. Chem. Int. Ed.* **56**, 7074–7077 (2017).

9. Silva, D. A., Stewart, L., Lam, K. H., Jin, R. & Baker, D. Structures and disulfide cross-linking of de novo designed therapeutic mini-proteins. *Febs. J.* **285**, 1783–1785 (2018).
10. Koder, R. L. et al. Design and engineering of an O₂ transport protein. *Nature* **458**, 305–309 (2009).
11. Smith, B. A. & Hecht, M. H. Novel proteins: from fold to function. *Curr. Opin. Chem. Biol.* **15**, 421–426 (2011).
12. Faiella, M. et al. An artificial di-iron oxo-protein with phenol oxidase activity. *Nat. Chem. Biol.* **5**, 882–884 (2009).
13. Watkins, D. W. et al. Construction and in vivo assembly of a catalytically proficient and hyperthermostable de novo enzyme. *Nat. Commun.* **8**, 358 (2017).
14. Cordova, J. M., Noack, P. L., Hilcove, S. A., Lear, J. D. & Ghirlanda, G. Design of a functional membrane protein by engineering a heme-binding site in glycophorin A. *J. Am. Chem. Soc.* **129**, 512–518 (2007).
15. Korendovych, I. V. et al. De novo design and molecular assembly of a transmembrane diporphyrin-binding protein complex. *J. Am. Chem. Soc.* **132**, 15516–15518 (2010).
16. Mahajan, M. & Bhattacharjya, S. Designed di-heme binding helical transmembrane protein. *Chembiochem* **15**, 1257–1262 (2014).
17. Kodali, G. et al. Design and engineering of water-soluble light-harvesting protein maquettes. *Chem. Sci.* **8**, 316–324 (2017).
18. Moffet, D. A. & Hecht, M. H. De novo proteins from combinatorial libraries. *Chem. Rev.* **101**, 3191–3204 (2001).
19. Lichtenstein, B. R. et al. Engineering oxidoreductases: maquette proteins designed from scratch. *Biochem. Soc. Trans.* **40**, 561–566 (2012).
20. Świerczek, M. et al. An electronic bus bar lies in the core of cytochrome bc₁. *Science* **329**, 451–454 (2010).
21. Chen, K., Huang, X., Kan, S. J., Zhang, R. K. & Arnold, F. H. Enzymatic construction of highly strained carbocycles. *Science* **360**, 71–75 (2018).
22. Kan, S. J., Lewis, R. D., Chen, K. & Arnold, F. H. Directed evolution of cytochrome c for carbon–silicon bond formation: bringing silicon to life. *Science* **354**, 1048–1051 (2016).
23. Rapson, T. D. et al. Design of silk proteins with increased heme binding capacity and fabrication of silk-heme materials. *J. Inorg. Biochem.* **177**, 219–227 (2017).
24. Krieg, S. et al. Heme uptake across the outer membrane as revealed by crystal structures of the receptor–hemophore complex. *Proc. Natl Acad. Sci.* **106**, 1045–1050 (2009).
25. Andersen, J. F. & Montfort, W. R. The crystal structure of Nitrophorin 2: a trifunctional antihemostatic protein from the saliva of *Rhodnius prolixus*. *J. Biol. Chem.* **275**, 30496–30503 (2000).
26. Mahajan, M. & Bhattacharjya, S. β -hairpin peptides: heme binding, catalysis, and structure in detergent micelles. *Angew. Chem.* **125**, 6558–6562 (2013).
27. D'Souza, A., Mahajan, M. & Bhattacharjya, S. Designed multi-stranded heme binding β -sheet peptides in membrane. *Chem. Sci.* **7**, 2563–2571 (2016).
28. D'Souza, A., Wu, X., Yeow, E. K. L. & Bhattacharjya, S. Designed heme-cage β -sheet miniproteins. *Angew. Chem.* **129**, 5998–6002 (2017).
29. Kortemme, T., Ramírez-Alvarado, M. & Serrano, L. Design of a 20-amino acid, three-stranded β -sheet protein. *Science* **281**, 253–2256 (1998).
30. Hughes, R. M. & Waters, M. L. Model systems for β -hairpins and β -sheets. *Curr. Opin. Struct. Biol.* **16**, 514–524 (2006).
31. Stanger, H. E. et al. Length-dependent stability and strand length limits in antiparallel β -sheet secondary structure. *Proc. Natl Acad. Sci.* **98**, 12015–12020 (2001).
32. Ottesen, J. J. & Imperiali, B. Design of a discretely folded mini-protein motif with predominantly β -structure. *Nat. Struct. Mol. Biol.* **8**, 535–539 (2001).
33. Zozulia, O., Dolan, M. & Korendovych, I. Catalytic peptide assemblies. *Chem. Soc. Rev.* **47**, 3621–3639 (2018).
34. Solomon, L. A., Kronenberg, J. B. & Fry, H. C. Control of heme coordination and catalytic activity by conformational changes in peptide–amphiphile assemblies. *J. Am. Chem. Soc.* **139**, 8497–8507 (2017).
35. Venkatraman, J., Shankaramma, S. C. & Balaram, P. Design of folded peptides. *Chem. Rev.* **101**, 3131–3152 (2001).
36. Antonini, E. & Brunori, M. Hemoglobin and myoglobin in their reactions with ligands. *Frontiers Biol.* **21**, 436 (1971).
37. Moore, G. R. & Pettigrew, G. W. *Cytochromes c: Evolutionary, Structural and Physicochemical Aspects* (Springer Science & Business Media, Berlin Heidelberg 2012).
38. Nastri, F. et al. A Heme–peptide metalloenzyme mimetic with natural peroxidase-like activity. *Chem. Eur. J.* **17**, 4444–4453 (2011).
39. Shinde, S., Cordova, J. M., Woodrum, B. W. & Ghirlanda, G. Modulation of function in a minimalist heme-binding membrane protein. *J. Biol. Inorg. Chem.* **17**, 557–564 (2012).
40. Li, L.-L. et al. Rational design of artificial dye-decolorizing peroxidases using myoglobin by engineering Tyr/Trp in the heme center. *Dalton Trans.* **46**, 11230–11238 (2017).

Acknowledgements

This work was supported by grants (RG 11/12, ARC 18/13) from the Ministry of Education (MOE), Singapore.

Author contributions

A.D., S.B. conceived the project, designed experiments, and analyzed data. A.D. performed all the experiments except IR. J.T. performed IR experiments. A.D., J.T. and S.B. wrote the manuscript. All authors commented on the manuscript.

Additional information

Supplementary Information accompanies this paper at <https://doi.org/10.1038/s42004-018-0078-z>.

Competing interests: The authors declare no competing interests.

Reprints and permission information is available online at <http://npg.nature.com/reprintsandpermissions/>

Publisher's note: Springer Nature remains neutral with regard to jurisdictional claims in published maps and institutional affiliations.



Open Access This article is licensed under a Creative Commons Attribution 4.0 International License, which permits use, sharing, adaptation, distribution and reproduction in any medium or format, as long as you give appropriate credit to the original author(s) and the source, provide a link to the Creative Commons license, and indicate if changes were made. The images or other third party material in this article are included in the article's Creative Commons license, unless indicated otherwise in a credit line to the material. If material is not included in the article's Creative Commons license and your intended use is not permitted by statutory regulation or exceeds the permitted use, you will need to obtain permission directly from the copyright holder. To view a copy of this license, visit <http://creativecommons.org/licenses/by/4.0/>.

© The Author(s) 2018